Received: 13 June 2016 | Accepted: 5 March 2017

DOI: 10.1002/hyp.11168

WILEY

RESEARCH ARTICLE

Influence of the El Niño/Southern Oscillation on South Korean streamflow variability

Jai Hong Lee | Pierre Y. Julien

Department of Civil and Environmental Engineering, Colorado State University, Fort Collins, CO 80523, USA

Correspondence
Jai Hong Lee, Department of Civil and Environmental Engineering, Colorado State University, Fort Collins, CO 80523, USA.
Email: june.lee@colostate.edu

Abstract

Deciphering the mechanisms through which the El Niño/Southern Oscillation (ENSO) affects hydrometeorological parameters in the tropics and extratropics is of great interest. We investigate climatic teleconnections between warm or cold phases of ENSO and streamflow patterns over South Korea using an empirical methodology designed to detect regions showing a strong and consistent hydroclimatic signal associated with ENSO. We calculate not only spatial coherence values by monthly streamflow composite formed over 2-year ENSO cycle and the first harmonic fit to detect candidate regions but also temporal consistency rates by aggregate composite and index time series to determine core regions. As a result, the core regions, namely, the Han river basin and the Nakdong river basin, are detected with a high level of response of ENSO phenomena to streamflow patterns. The ENSO composites for both core regions indicate drier (wetter) conditions in early autumn of the warm (cold) episode years and wetter (drier) conditions from winter to spring of the following year. For both regions, the spatial coherences are over 92% (82%) and the temporal consistencies are 71% (75%) during the El Niño (La Niña) events. In addition, for the core regions identified by composite-harmonic analysis for both extreme episodes, the results of comparative analyses by using correlation, annual cycle, and Wilcoxon rank sum test indicate that 2 opposite phases-streamflow relationships have a tendency of sign reversal of the streamflow anomaly. Also, the positive departures during the El Niño years show more coherent and strong responses than the negative anomalies in the La Niña events. In conclusion, South Korea experiences climatic teleconnection between ENSO forcing and midlatitude streamflow patterns.

KEYWORDS

ENSO, Southern Oscillation, streamflow

1 | INTRODUCTION

The El Niño/Southern Oscillation (ENSO) has been one of the most widely studied topics due to the fact that the extreme phases of ENSO are usually associated with major hydrologic extremes such as floods and droughts in many regions throughout the world. In the global and regional scale studies, significant relationships have been reported between the tropical ocean-atmospheric ENSO forcing and hydrometeological variables such as precipitation, temperature, wind, and streamflow in the tropics and extratropics. Since the first investigation of Walker (1923) on the influence of the Southern Oscillation (SO) on rainfall fluctuations by Indian monsoon, many global scale studies focused on the evolution of ENSO cycle indicated noticeable climatic links between hydrometeorological parameters and both phases of the SO throughout the world. Berlage (1966), Stoeckenius (1981), Pan and Oort (1983), and Rasmusson and Wallace (1983) investigated climatic relationships between the ENSO cycle and meteorological anomalies on a global basis. Also, Ropelewski and Halpert (1989; hereafter abbreviated as RH); Kiladis and Diaz (1989; hereafter designated as KD); and Bradley, Diaz, Kiladis, and Eischeid (1987) pointed out notable ENSO-related signals with the identification of spatial patterns and time series showing a statistically significant correlations between both phases of the remote ENSO forcing and precipitation and temperature patterns throughout the various parts of the world.

Meanwhile, the regional scale works for low and middle latitude relating the remote ENSO cycle to hydroclimatic variations by Douglas and Englehart (1981); Ropelewski and Halpert (1986); Schonher and

Nicholson (1989); Grimm, Ferraz, and Gomes (1998); Price, Stone, Huppert, Rajagopalan, and Alpert (1998); and Karabörk and Kahya (2003) revealed statistically significant correlation between regional precipitation and ENSO forcing. Douglas and Englehart (1981) and Ropelewski and Halpert (1986) revealed that the southeastern United States has a tendency for positive winter precipitation anomalies for the ENSO event years, as well as Ropelewski and Halpert (1987, 1989) and Kiladis and Diaz (1989) investigated the statistically significant correlation between two opposite phases of ENSO and precipitation patterns over North America. In addition, some studies for midlatitude regions pointed out the distinct behavior of the ENSO-related streamflow anomalies. Cayan and Peterson (1989), Cayan and Webb (1992), Redmond and Koch (1991), and Diaz and Kiladis (1993) investigated the teleconnection of North Pacific atmospheric circulation and the western United States streamflow, and Kahya and Dracup (1993, 1994) and Dracup and Kahya (1994) diagnosed the responses of U.S. streamflow patterns to remote ENSO forcing in the light of midlatitude teleconnections driven by the oscillation of sea surface temperature over tropical Pacific Ocean. Chiew, McMahon, Dracup, and Piechota (1994) described the climatic links between ENSO and streamflow patterns in south-east Australia with an empirical methodology, and Kahya and Karabörk (2001) examined statistically significant regions having spatially coherent and temporally consistent response of streamflow patterns in Turkey to both phase of ENSO. In Asian regions, the study by Chandimala and Zubair (2007) provided the predictability of Kelani river streamflow in conjunction with remote ENSO forcing and sea surface temperature (SST) by means of empirical orthogonal functions and correlation analysis. Zhang, Xu, Jiang, and Wu (2007) confirmed variability and teleconnections between Yangtze River basin streamflow and the extreme phases of SO by cross-wavelet and wavelet coherence. Kashid, Ghosh, and Maity (2010) examined hydroclimatic teleconnections between large-scale circulation patterns and streamflow in Mahanadi River, India, using statistical techniques and artificial intelligence tools.

Several recent studies for South Korea (e.g., Cha, Jhun, & Chung, 1999; Lee, 1999; and Shin, 2002) have suggested statistically strong and consistent responses of hydrometeorological variation to the remote ENSO forcing. In the diagnostic investigation on Korean climate variations for ENSO year, Cha et al. (1999) described the evolving feature of climate in South Korea with the extreme phases of ENSO using synoptic data and European Centre for Medium-Range Weather Forecasts (ECMWF) grid data. Lee (1999) investigated the relationship between ENSO and drought in Korea using the cross correlation analysis with Palmer drought severity index and nine ENSO indicators, and Lee and Julien (2015, 2016) revealed that two phases of the remote ENSO forcing are the dominant drivers of precipitation and temperature fluctuations over South Korea based on harmonic and correlation analysis. Shin (2002) applied correlation analysis to Korean precipitation patterns and the tropical ENSO cycles in order to show climatic teleconnection between the tropical thermal forcing and hydrologic extremes such as floods and droughts. Jin, Kawamura, Jinno, and Berndtsson (2005) calculated Kendall's and Pearson's correlation analyses between the SO index (SOI) categorized according to magnitude and monthly precipitation data converted into cubic root or nonexceedance probability at two stations in Korea and Japan and provided evidence of teleconnection between ENSO and regional hydrological variables.

As seen from the above, almost all aforementioned regional and global papers concentrate on the Pacific Rim countries such as Australia, India, and the United States. Also, these studies have focused on mostly the warm ENSO events as a source of large-scale ocean-atmospheric circulation due to the fact that the cold ENSO events are less distinct and causes less hydrologic extremes, for example, floods and droughts, than the El Niño phase. Hence, there is no global scale study in the literature concerning the climate impacts of both phases of the ENSO events on streamflow pattern. Furthermore, the influence of ENSO on the East Asian climatology is not limited to the warm phase of the ENSO episodes, as well as increasingly, the potential researches of climatic teleconnections are asking for more information about the overall features of the hydrometeorological impacts modulated by ENSO. Thus, it is necessary to investigate systematically how both phases of the ENSO cycle affect hydrometeorological parameters in the East Asian regions. In the global scale analysis, Ropelewski and Halpert (1987, 1989) revealed strong and consistent ENSO-related precipitation signals for several regions including the East Asia. From the visual inspection of the global scale vectorial maps in the aforementioned papers, the statistically significant signals of ENSO-precipitation relationship are not clearly identified in Korean Peninsula because of station coverage limitations. In the present study, we motivate expansion of previous work by a diagnostic investigation of the influences of the ENSO on the streamflow patterns over South Korea with respect to both phases of the ENSO events, using adequate and sufficient dataset.

The present study mainly aims to explore significant climatic relationships between both phases of the ENSO events and South Korean streamflow patterns by means of composite-harmonic analysis designed to describe hydroclimatic signals in terms of the amplitude and phase of ENSO–streamflow teleconnection, to evaluate the spatial coherence and temporal consistency of ENSO-related streamflow signals in association with the phases of the ENSO episodes, and to perform the comparative interpretation of two opposite phases-streamflow signals in terms of magnitude and sign of the correlations, through comparative analyses by using correlation, annual cycle, and Wilcoxon rank sum (WRS) test (Trauth, 2015).

2 | DATA

The present study is based on monthly streamflow amounts derived from all gaging stations distributed in several major river basins throughout South Korea. The dataset was obtained from Korea Annual Hydrological Report published by Ministry of the Land, Infrastructure and Transport, which is in charge of the flood forecast, hydrological observation, and hydrological data management overall Korean river basins. The time series cover more than 14 (12) extreme events of El Niño (La Niña) extending from 1962 through 2014. The observational records are selected only if they have less than a month missing data, as well as each monthly streamflow data cover 53 years of observation between the years 1962 and 2014

spanning at least 12 ENSO episodes. Accordingly, 60 stations were applied in our current analysis in consideration of the temporal and spatial persistency.

For the purpose of identifying a consistent response of South Korean streamflow variation to the remote ENSO forcing, we selected 14 El Niño episodes and 12 La Niña episodes following the definitional approach of Quinn, Zopf, Short, and Kuo Yang (1978); Ropelewski and Halpert (1987, 1989); Kiladis and Diaz (1989); and Trenberth (1997). Ropelewski and Halpert (1987, 1989) applied the list of extreme episodes of Quinn et al. (1978) based on SST data near the South American coast (4°S to 12°S). Kiladis and Diaz (1989) defined the ENSO events using a standard SO combined with an SST anomaly index for the eastern Pacific (4°N to 4°S, 130°W to the South American coast). Also, Trenberth (1997) based their definition on the extreme events for which the 5-month running means of the monthly SST anomalies averaged for the Nino 3 region (5°N–5°S, 150°–90°W) are +0.5 °C or more for at least six consecutive months. Taking into account the differences among various methodological approaches in defining El Niño and La Niña events, a wide set of the events qualified by a comprehensive range of criteria as mentioned above was applied regardless of particular sorts of events. Table 1 indicates the total episodes of extreme phases of ENSO applied in this analysis.

As an approach of describing atmospheric variation over the tropical Pacific Ocean, the SOI, which is one of the large-scale climatic signals, was applied. The SOI, as an atmospheric pressure-based climate indicator, is usually computed using Darwin–Tahiti mean sea lever pressure difference based on standardized index with zero mean and unit standard deviation. In this present analysis, we employed the time series of SOI calculated by the National Oceanic Atmospheric Administration Climate Prediction Center (http://www.cpc.ncep.noaa.gov/data/indices/soi).

3 | ANALYSIS

The overall methodology used in this present analysis, which is following the comprehensive empirical approach by Ropelewski and Halpert (1986), is outlined in the schematic description of Figure 1. The detailed procedures of the analysis method can be briefly summarized as follows. The first step is to convert the original data to monthly and seasonal-based time series, for example, transformation of monthly streamflow data into standardized streamflow index (SSI), seasonal nonexceedance probability time series, classification of seasonal SOI, and modular coefficients; the next step is to carry out composite-harmonic analysis for determination of spatially coherent and temporally consistent core regions; and the final step is to perform comparative analysis by means of correlation, annual cycle, and the WRS test in order for the comparative interpretation of two opposite phases-streamflow signals in terms of magnitude and sign of the correlations.

Prior to the composite-harmonic analysis to examine the ENSO–streamflow teleconnection, we converted the streamflow data to SSI, which was coined to describe the modification of standardized precipitation index with some changes and additions. The standardized precipitation index is a drought measuring index, which was formulated for effective assessment and monitoring of wet and dry condition by McKee, Doesken, and Kleist (1993). The SSI calculating procedures are outlined below based on the approach of McKee et al. (1993).

1. The monthly streamflow data of 60 stations are transformed into the time series based on gamma distribution fit to the data of each month.
2. The fitted frequency distribution is converted to cumulative distribution function of the standard normal distribution based on equal probability.
3. The SSI dataset, which is subjected to the composite-harmonic process, can be computed by means of the standard deviations obtained from the above cumulative distribution function with zero mean and unit variance.

The SSI is very straightforward to estimate due to the fact that the one variable is used as input data, as well as very easy to compare from a spatial and temporal viewpoint because the index is presented as dimensionless values. Furthemore, Guttman (1998) indicated that the SSI index is useful and conducive to statistical data process.

As a follow-up to the composite analysis by Ropelewski and Halpert (1986), which is a methodology to represent the climatic pattern of the ENSO–streamflow relationship, ENSO composites of the SSI time series for all stations are formed on the 2-year cycle basis, which is composed of July (−) to December (−) representing the preceding years of the episodes, January (0) to December (0) designating the event years, and January (+) to June (+) indicating the following year of the events. The final ENSO composites structure is produced by averaging the transformed SSI time series for all ENSO events. This idealized 2-year ENSO composite is used as an input data of harmonic analysis, which is one of the objective mathematical procedures to describe seasonal climate variabilities based on the superposition of waves and generalization of the Fourier functions (Horn & Bryson, 1960). The inset diagram of Figure 2 indicates four harmonic fits for annual variation of monthly SSI data based on Scott and Shulman (1979). Under the assumption that only one extreme streamflow value is corresponded to the warm and cold phases of ENSO phenomena, we confined the only first harmonic for the ENSO composite. The following are the formulas for the harmonic analysis (Wilks, 1995).

TABLE 1 List of the ENSO episode years included in this study

El Niño years	La Niña years
1963, 1965, 1969, 1972, 1976, 1982, 1986, 1991, 1994, 1997, 2002, 2004, 2006, 2009.	1964, 1971, 1973, 1975, 1985, 1988, 1995, 1998, 2000, 2005, 2007, 2010.

Note. ENSO = El Niño/Southern Oscillation.

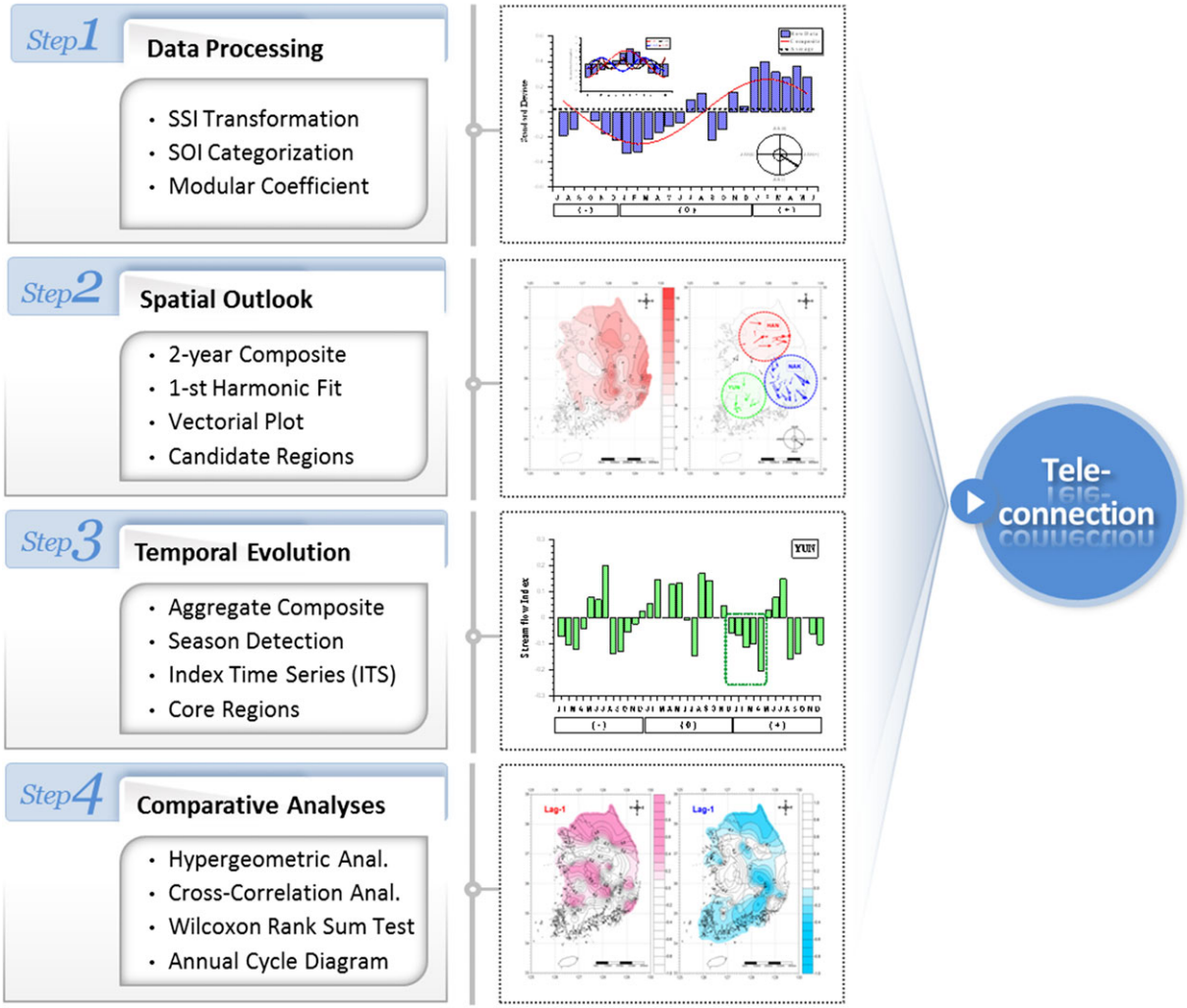

FIGURE 1 Flowchart of the empirical methodology

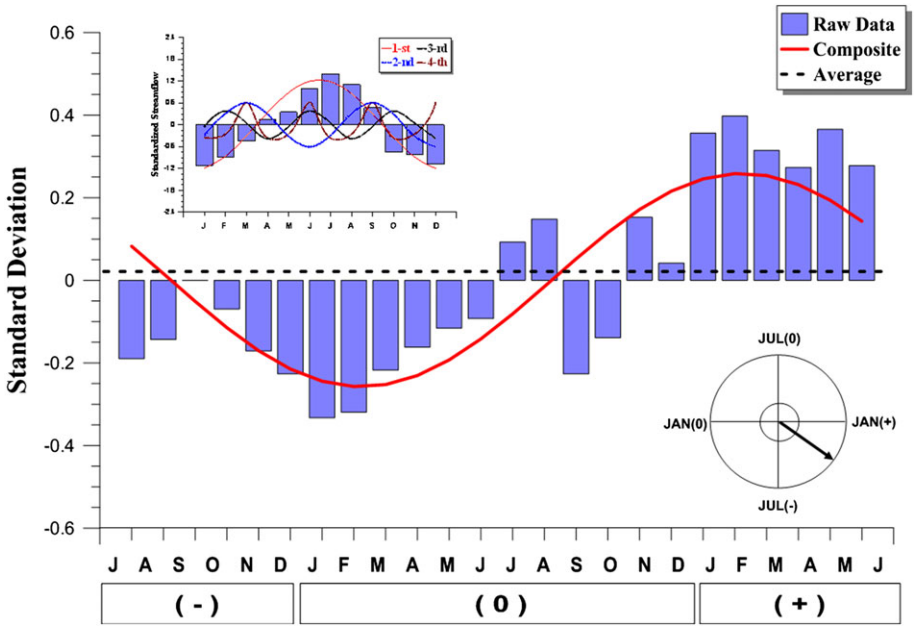

FIGURE 2 A first harmonic fit to the streamflow El Niño composite for the gauging station NAK.25. The amplitude and the phase of the first harmonic are presented as a harmonic dial (the lower right). The inset diagram (the upper left) depicts an example illustrating several harmonic fits of annual cycle for monthly streamflow (standardized streamflow index) from the first to the fourth harmonic

$$SSI_t = \overline{SSI} + \sum_{k=1}^{T/2}\left[X_k cos\left(\frac{2\pi kt}{T}\right) + Y_k sin\left(\frac{2\pi kt}{T}\right)\right] = \overline{SSI} + \sum_{k=1}^{N/2}\left[Z_k cos\left(\frac{2\pi kt}{T} - \theta_k\right)\right], \quad (1)$$

where

$$X_k = \frac{2}{T}\sum_{t=1}^{T} SSI_t cos\left(\frac{2\pi kt}{T}\right), \quad Y_k = \frac{2}{T}\sum_{t=1}^{N} SSI_t sin\left(\frac{2\pi kt}{T}\right) \quad (2)$$

$$\theta_k = tan^{-1}\frac{Y_k}{X_k}(X_k > 0), \quad \frac{\pi}{2}(X_k = 0), \quad tan^{-1}\frac{Y_k}{X_k} \pm \pi\ (X_k < 0), \quad (3)$$

where SSI_t is the SSI value at t, $\overline{SSI}$ is the average SSI value, k is the harmonic index, T is the total period, Z_k is the amplitude, $(X_k{}^2 + Y_k{}^2)^{0.5}$, θ_k is the time of maximum deviation (phase shift), and X_k and Y_k are the Fourier coefficients. It should be noted that the amplitude and phase of harmonic waves represent strength and time of the ENSO-related streamflow signal (Figure 2).

The amplitude and phase of the first harmonic are plotted as harmonic vectors with the length and direction on a vectorial map providing evidence of candidate geographic boundary that has a coherent ENSO response. This harmonic dial map provides evidence of a candidate region of spatially coherent ENSO-related streamflow signal by identifying a similar group of harmonic vectors in terms of amplitude and angular orientation. In order to determine the candidate regions, the spatial coherence rate (R_{sc}) is employed following the calculation of Ropelewski and Halpert (1986, 1987).

$$R_{sc} = \frac{\overline{V}}{S} = \frac{\left[(\sum V cos\,\beta)^2 + (\sum V sin\,\beta)^2\right]^{0.5}/N}{\sum V/N}, \quad (4)$$

where $\overline{V}$ is the mean value of vectors within candidate regions, S is the mean value of each vector magnitude, V, β, and N are the magnitude, phase, and total number of vectors. Following the suggestion of Ropelewski and Halpert (1986), a candidate region is limited to regions for which the R_{sc} is equal to or exceeds 0.8.

For the purpose of detection of signal season having statistically significant relationship between the remote ENSO cycle and local streamflow variation, we formed aggregate composites by means of spatial averages of the ENSO composites within the candidate regions. Plotting these aggregate composites on a basis of a 3-year period provides a better representation of signal season and coverage of the ENSO life cycle (Kahya & Dracup, 1993). From the visual inspection of the aggregate composite, we can find signal season within the ENSO cycle, which has a period of four or more consecutive months with the same signal. For the detected seasons, another time series of streamflow data, that is, index time series (ITS), are employed to quantify temporally consistent response of streamflow pattern to the remote ENSO forcing. The ITS is extracted by spatially averaging streamflow data of all stations as well as by temporally averaging all observational periods. Accordingly, in order for the determination of

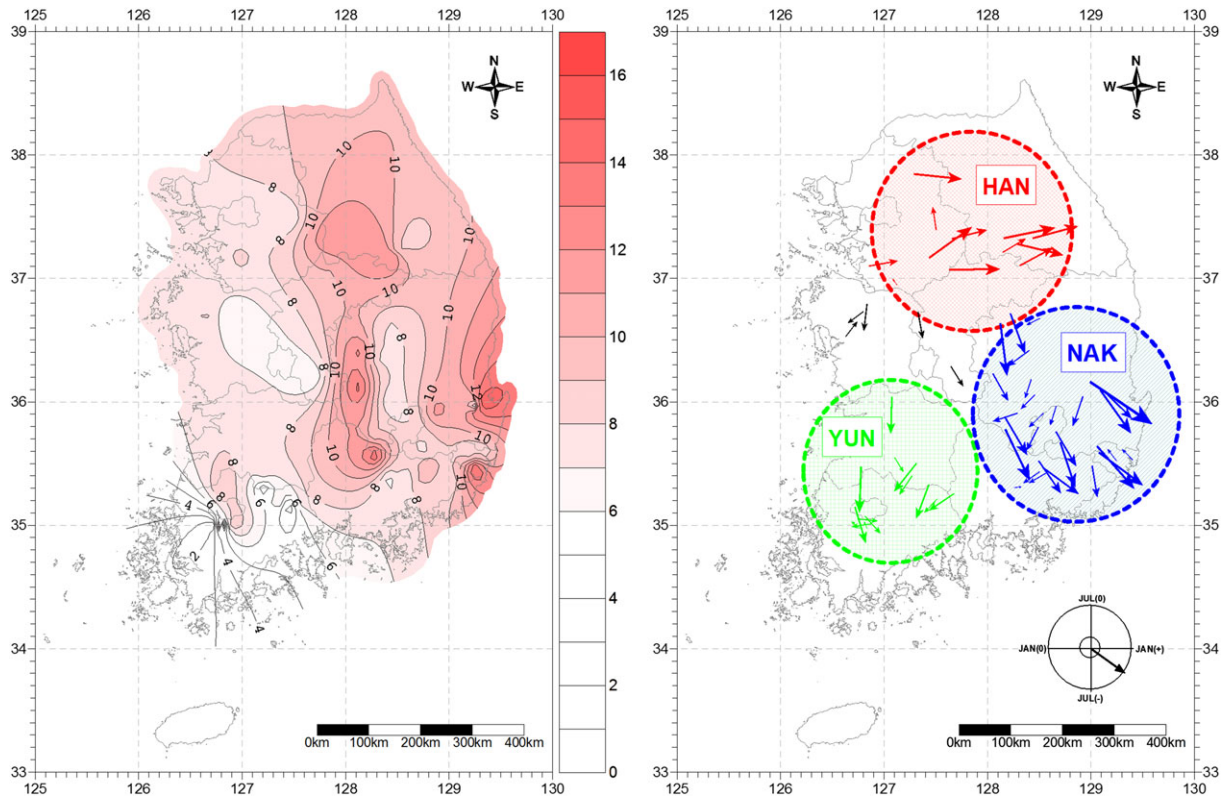

FIGURE 3 Contour map (left) and vectorial map (right) based on the first harmonic of the 2-year El Niño composites. Scale for the direction of arrows: south, July(−); west, January(0); north, July(0); and east, January(+). The magnitude of arrows is proportional with the amplitude of the harmonics

TABLE 2 Properties of the candidate regions (El Niño events)

Region	Coherence	Season	Total episode	Occur. episode	Consistency
HAN	0.92	Dec(0)–May(+)	14	10	0.71
NAK	0.95	Jan(+)–May(+)	14	10	0.71
YUN	0.72	–	–	–	–

Note. HAN = Han; NAK = Nakdong; YUN = Youngsan.

core regions showing a consistent correlation between the remote ENSO forcing and streamflow pattern within the previously detected candidate regions, we calculated the temporal consistency rate (R_{tc}), which is the ratio of the number of years showing the ENSO–streamflow relationship within the ITS cycle to the number of total event years.

Following the approach of Kahya and Dracup (1994), we counted the number of occurrences of extreme streamflow events in association with the remote ENSO forcing to identify the climatic relationship between ENSO and the extreme phase of streamflow. To determine the limits of the extreme states, we ranked the ITS values in decreasing order of magnitude, normalized by the amount of the total data, and obtained the probability through probability plotting position method. The limits for the highest (lowest) index are assigned a probability of ITS equal to 80% (20%).

For the purpose of estimating the statistical significance of correlation of the ENSO phenomena and streamflow variation, we employed the hypergeometric distribution method, which is an effective method for estimating the cumulative probability of the chance of occurrence of the ENSO-related signal season at random. For the hypergeometric distribution model, the cumulative probability, that is, the occurrence of at least m successes out of n trials in N population size including k successes, can be estimated following the analysis of Haan (1977).

$$Fx(m,N,n,k) = \sum_{i=m}^{n} \binom{k}{i}\binom{N-k}{n-i} / \binom{N}{n} \quad (5)$$

For this probability distribution model, we tested two cases, I and II, depending on the context of a success. We defined that of case I as the observation of above (below) normal streamflow anomaly in the ITS, and for case II as the occurrence of extremely wet (dry) condition whose the positive (negative) anomaly is greater (smaller) than the 80% (20%) value in the ITS based on the approach of Kahya and Dracup (1994).

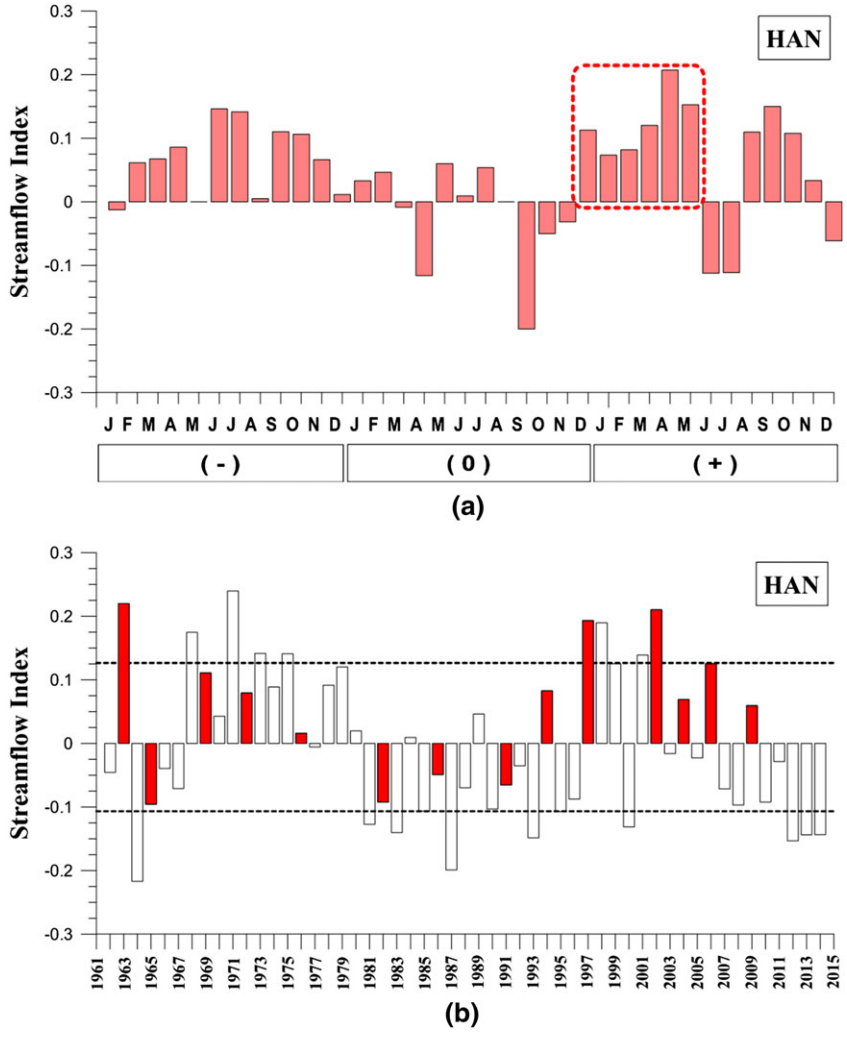

FIGURE 4 (a) El Niño aggregate composite for the candidate HAN region. The dashed line box delineates the season of possible El Niño-related responses. (b) The index time series for the HAN region for the season previously detected. El Niño years are shown by solid and red bars. The dashed horizontal lines are the upper (80%) and lower (20%) limits for the distribution of index time series values

In order for comparison between both impacts of the warm and cold phases of ENSO on streamflow fluctuation, we calculated correlation coefficients for the SOI and the SSI on a seasonal basis through lag-correlation analysis. From this calculation, the strength and sign of the ENSO–streamflow teleconnection are evaluated using the resulting correlation coefficients. Prior to calculating correlation coefficients, seasonal time series for the SOI and streamflow data are established based on 3-month averaged seasons, such as MAM for March to May, JJA for June to August, SON for September to November, and DJF for December to February. Meanwhile, seasonal streamflow data are converted to nonexceedance probability time series with respect to each season to minimize disparities among stations and periodicities in time series. The entire streamflow data are ranked in increasing order of magnitude and sequently provide the associated probability through normalization and nonparametric approach such as Weibull method. Additionally, following the suggestion of Jin et al. (2005), we classified the SOI time series into five levels depending on the magnitudes of each value, for example, El Niño (strong phase, SOI<−2, and weak phase, −2≤SOI<−1), La Niña (weak phase, 1<SOI≤2, and strong phase, SOI>2), and normal phase (−1≤SOI≤1).

As a nonparametric test for comparing between both responses of streamflow variation to the opposite phases of ENSO cycle, we used the WRS test which is designed to assess differences between two groups of datasets. The two datasets are collected with respect to the warm and cold events with the alternative hypothesis being that one dataset is stochastically different from, that is, greater or smaller than, the other, and with the null hypothesis of the equality of the two datasets. In this test, modular coefficients, that is, the rate of the individual streamflow value to the mean value of the total data series, are employed. From the above WRS test, we can identify whether two phases of ENSO–streamflow signals are equal or not.

In order to compare the intensity and seasonal behavior of the 3-year ENSO composite and annual streamflow fluctuations, we plotted an annual cycle diagram for both event years and entire observation period following the approach of Kahya and Dracup (1993) and Karabörk and Kahya (2003). For this comparison, each monthly streamflow data within the core region are transformed into modular coefficients to mitigate the effect of disperse factors of mean and variance in original station data, through which streamflow fluctuation can be represented in terms of the percent of annual mean value. Then a regional monthly time series are extracted by computing the rate of original value to annual mean value for total records and spatially averaging the modular coefficients for all stations. From these resulting time series, an annual cycle diagram for ENSO composites and

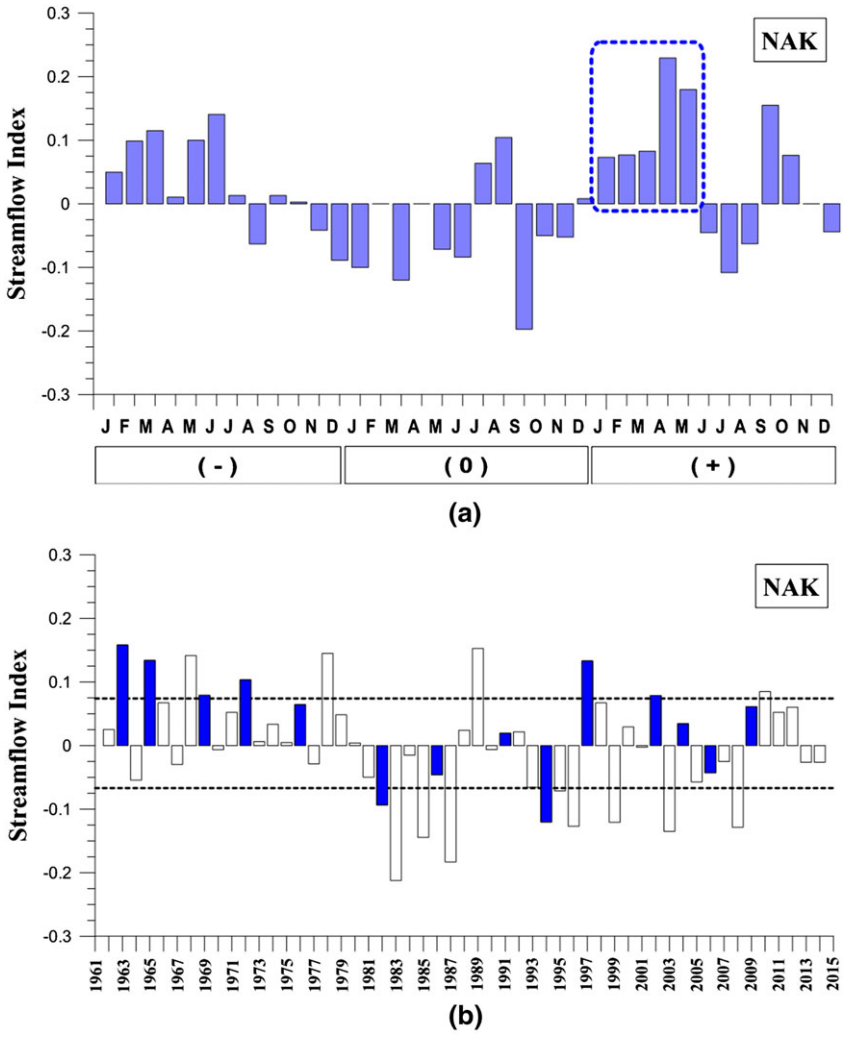

FIGURE 5 As in Figure 4, except for the candidate NAK region and El Niño years are shown by solid and blue bars

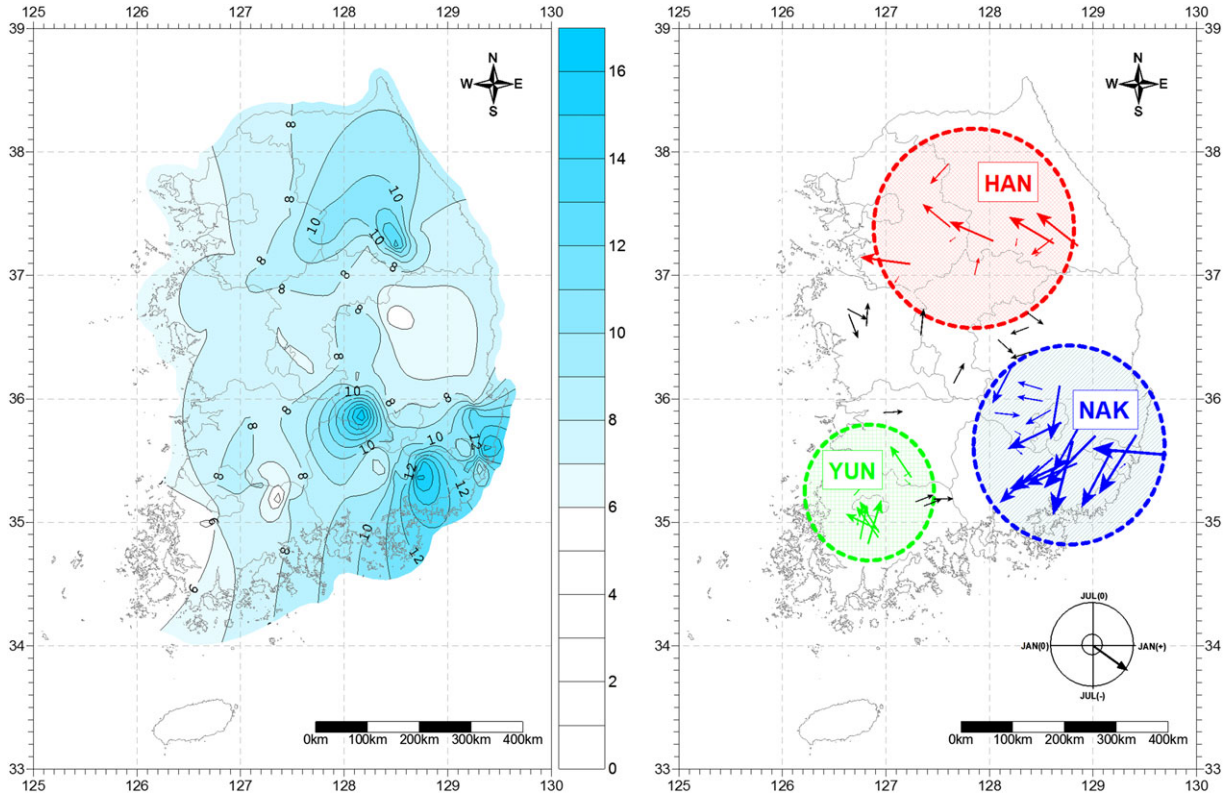

FIGURE 6 As in Figure 3, except for La Niña composites

streamflow variation is plotted on a 3-year basis to identify the evidence that the ENSO forcing modulates the streamflow fluctuation by increasing or decreasing trend.

4 | RESULTS

As a result for the El Niño-related streamflow response, Figure 3 indicates the spatial outlook of the resulting candidate regions expressed by the contour and vectorial map plotted through the composite-harmonic analysis. From the previously plotted contour and vectorial map, the entire area is classified into three candidate regions, for example, the Han river basin (HAN), the Nakdong river basin (NAK), and the Youngsan river basin (YUN). Then, the general results of the composite-harmonic analysis are outlined in Table 2 describing two core regions out of three candidate regions based on the spatial coherence rate (R_{sc}) and the temporal consistency rate (R_{tc}). The first column represents the candidate regions; the second, the spatial coherence rate (R_{sc}); the third, the signal seasons; the fourth to sixth, and the overall consistency evaluation with the temporal consistency rate (R_{tc}).

TABLE 3 As in Table 2, except for La Niña events

Region	Coherence	Season	Total episode	Occur. episode	Consistency
HAN	0.82	Dec(0)–Apr(+)	12	9	0.75
NAK	0.86	Nov(0)–May(+)	12	9	0.75
YUN	0.70	–	–	–	–

Note. HAN = Han; NAK = Nakdong; YUN = Youngsan.

For the Han river basin (HAN), the spatial coherence value (R_{sc}) is equal to 92%. From the aggregate composite diagram for El Niño events in Figure 4(a), the subsequence of above normal streamflow from December (0) to May (+) is detected as apparent ENSO signal season representing a consistent El Niño–streamflow teleconnection as highlighted by the dashed box in Figure 4(a), which is subject to following calculation of temporal consistency for the relationship. This signal season indicates a tendency for greater than average streamflow for 10 out of 14 ENSO events, which is a relatively high level of temporal consistency rate (R_{tc}) as shown in Figure 4(b). Also, out of the nine occurrences exceeding the 80% ITS value, that is, the highest limit of the time series, four of them are coincident with the warm extreme phase of ENSO as shown by the dashed horizontal line in Figure 4(b). These findings indicate that the Han river basin (HAN) is identified as a core region showing the noticeable climatic link between the remote El Niño forcing and regional streamflow fluctuations.

In the Nakdong river basin (NAK), the spatial coherence rate (R_{sc}) is computed as 95%. As a result of the aggregate composite for the warm episodes of ENSO in Figure 5(a), the time period between January (+) and May (+) is identified as a signal season showing a well-pronounced and consistent impact of the ENSO forcing on regional streamflow variations, which is outlined by dashed box. The streamflow time series for signal season show that 10 positive anomalies out of 14 are in association with the remote El Niño forcing at a high rate of temporal consistency rate (R_{tc}) as depicted in Figure 5(b). On a basis of the ITS values higher than the upper limit (80%), six out of 10 wettest years occur in accordance with the warm event years, which is highlighted by the dashed lined in Figure 5(b). From the above results based on the spatial coherence and temporal consistency for ENSO–Streamflow

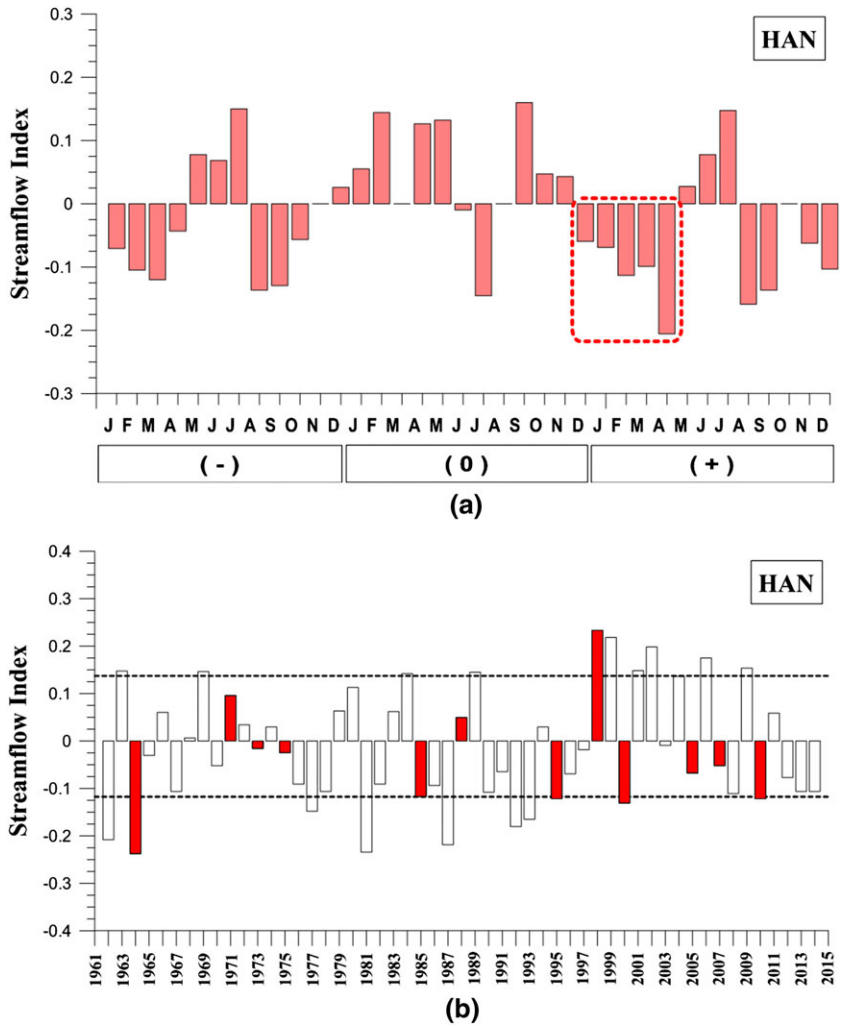

FIGURE 7 La Niña aggregate composite for the candidate HAN region. The dashed line box delineates the season of possible La Niña-related responses. (b) The index time series for the HAN region for the season previously detected. La Niña years are shown by solid and red bars. The dashed horizontal lines are the upper (80%) and lower (20%) limits for the distribution of index time series values

teleconnection, the Nakdong river basin (NAK) is considered as a core region.

On the other hand, in the Youngsan river basin (YUN), the spatial coherence rate (R_{sc}) is equal to 72%, which is not acceptable taking the aforementioned criterion into consideration. Furthermore, from the inspection for the aggregate composite diagram and the ITS plot, any consistent seasonal signal of El Niño–streamflow teleconnection was not detected. As a result, these findings suggest that the Youngsan river basin (YUN) is hard to be accepted as a core region in association with the remote El Niño forcing.

The same analysis is performed for the cold phase of ENSO forcing. For the La Niña–streamflow relationship, the contour and vectorial map based on the composite-harmonic analysis are showed in Figure 6 with the resulting candidate regions. From the above contour and vectorial map, three candidate regions are detected, for example, the Han river basin (HAN), the Nakdong river basin (NAK), and the Youngsan river basin (YUN). Accordingly, the results of the composite-harmonic analysis are outlined in Table 3 with identification of two core regions out of three candidate regions based on the spatial and temporal consistency rate (R_{sc} and R_{tc}).

In the Han river basin (HAN), the spatial coherence rate (R_{sc}) is computed as 82%. As a result of the aggregate composite for the cold episodes of ENSO in Figure 7(a), the time period between December (0) and April (+) is identified as a signal season showing a well-pronounced and consistent impact of the ENSO forcing on regional streamflow variations, which is outlined by dashed box. The streamflow time series for signal season show that nine negative departures out of 12 are in association with the remote La Niña forcing at a high rate of temporal consistency rate (R_{tc}) as depicted in Figure 7(b). On a basis of the ITS values lower than the lowest limit (20%), four out of 10 driest years occur in accordance with the cold event years, which is highlighted by the dashed lined in Figure 7(b). From the above results based on the spatial coherence and temporal consistency for ENSO–streamflow teleconnection, the Han river basin (HAN) is considered as a core region.

For the Nakdong river basin (NAK), the spatial coherence value (R_{sc}) is equal to 86%. From the aggregate composite diagram for La Niña events in Figure 8(a), the subsequence of below normal streamflow from November (0) to May (+) is detected as apparent ENSO signal season representing a consistent La Niña–streamflow teleconnection as highlighted by the dashed box in Figure 8(a), which is subject to following calculation of temporal consistency for the relationship. This signal season indicates a tendency for smaller than average streamflow for nine out of 12 ENSO events, which is a relatively high level of temporal consistency rate (R_{tc}) as shown in Figure 8(b). Also, out of the 10 occurrences less than the 20% ITS value, that is,

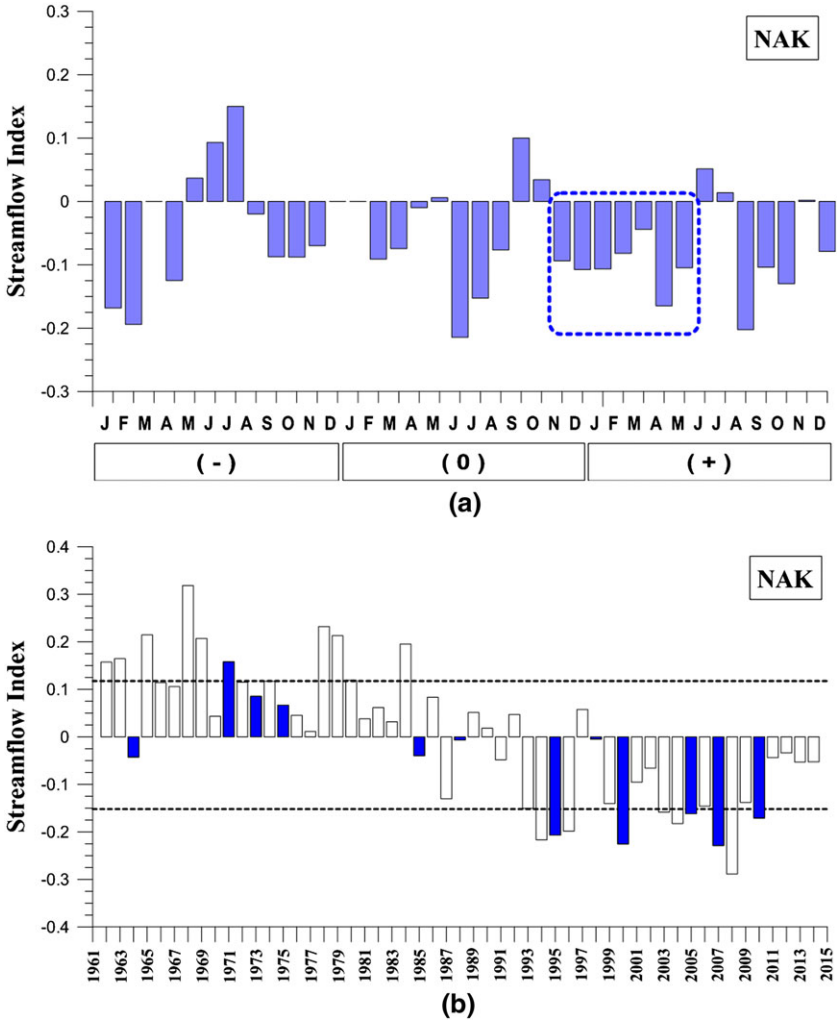

FIGURE 8 As in Figure 7, except for the candidate NAK region and La Niña years are shown by solid and blue bars

the lowest limit of the time series, five of them are coincident with the cold extreme phase of ENSO as shown by the dashed horizontal line in Figure 8(b). These findings indicate that the Nakdong river basin (NAK) is identified as a core region showing the noticeable climatic link between the remote La Niña forcing and regional streamflow fluctuations.

In the Youngsan river basin (YUN), similar to the result for the El Niño episodes for this region, the spatial coherence rate (R_{sc}) is equal to 70%; furthermore, through the investigation for the aggregate composite diagram and the ITS plot, any statistically significant signal for La Niña–streamflow teleconnection was not detected. Accordingly, the Youngsan river basin (YUN) proved to be unacceptable as a core region with relation to the remote La Niña phenomena.

TABLE 4 Probabilistic assessments for significance level based on the hypergeometric distribution. The cumulative probability is the occurrence of at least *m* successes out of n trials in *N* population size including *k* successes

Events	Case	Region	*N*	*k*	*n*	*m*	Prob.
El Niño	I	HAN	53	24	14	10	0.019
		NAK	53	28	14	10	0.069
	II	HAN	53	9	9	4	0.030
		NAK	53	10	10	6	0.001
La Niña	I	HAN	53	30	12	9	0.095
		NAK	53	26	12	9	0.034
	II	NAK	53	10	10	4	0.065
		NAK	53	10	10	5	0.012

Note. HAN = Han; NAK = Nakdong; YUN = Youngsan.

The results from the hypergeometric distribution model in order to estimate the cumulative probability of random occurrences of the ENSO-related signal season in association with both extreme events are summarized in Table 4. For case I, both core regions, that is, the HAN region and the NAK region, demonstrate a significant relationship between the El Niño forcing and streamflow variations occurring at high rates of 98% and 93%, which are very low chance of random occurrence of the above normal streamflow departures. Then for case II, both core regions exhibited a fairly low chance occurring at random of the wettest streamflow anomalies exceeding the highest limit (80%) for the warm phase of ENSO resulting in over 97%. On the other hand, the cumulative probability of random occurrences of the below normal streamflow anomalies in association with the La Niña events for case I results in a quite low value for both core regions showing a significant relationship at a level of 90% and 97%. Also, for case II during the cold episodes, the results of hypergeometric distribution approach for the NAK regions show a very low chance of random occurrence of the driest streamflow departures less than the lowest limit (20%) with a lever of 99%, and that of the HAN regions is estimated as 93%. As a result, these outcomes from the hypergeometric distribution for both core

TABLE 5 Cross-correlation coefficients with respect to regions

Core region		Strong El Niño SOI				Strong La Niña SOI			
		Lag-1	Lag-2	Lag-3	Lag-4	Lag-1	Lag-2	Lag-3	Lag-4
El Niño	HAN	−0.07	0.38	0.08	**0.46**	−0.07	0.09	−**0.17**	0.01
	NAK	0.11	0.31	−0.23	**0.41**	0.09	0.04	−**0.09**	0.00
La Niña	HAN	0.32	**0.40**	0.27	0.19	0.02	0.15	−**0.21**	0.08
	NAK	−0.04	0.04	−0.03	**0.16**	−0.14	−0.07	−**0.26**	-0.15

Note. HAN = Han; NAK = Nakdong. SOI = Southern Oscillation Index. An underlined bold indicates the strongest correlation.

regions represent the similar results with a statistically significant level for positive and negative relationship.

Table 5 and Figure 9 indicate the overall results from lag-correlation analysis on a seasonal basis between the categorized SOI and the nonexceedance probability time series of streamflow variations to investigate the strength and sign of ENSO–streamflow correlation. The assumption that the time-series data are serially independent is identified to be valid through the temporal autocorrelation coefficient for the monthly anomaly time series. As a result, based on the 90% confidence level, the seasonal streamflow time series are not only correlated with the warm extreme events, but also with the cold phase of ENSO. For the strong El Niño SOI phase, the highest values of correlation coefficient in both regions range from 0.16 to 0.46 with lag-4 seasons except for the case of La Niña-HAN region (0.4 with lag-2), while the values of the strongest correlation for the strong La Niña phase are calculated as −0.09 to −0.26 with lag-3 seasons as highlighted by underline in Table 5. Accordingly, the overall results from the above lag-correlation analysis suggest that the stronger intensity of the extreme phase of ENSO, the larger the influence on South Korean streamflow fluctuation with the lag of 3 and 4 seasons.

As a follow-up to the methodological approach by Trenberth and Stepaniak (2001) and Kennedy, Garen, and Koch (2009), additional cross-correlation analysis is performed in order to examine the climate teleconnection between a large-scale climate index, that is, trans-Niño index (TNI), and the SSI. The TNI time series are classified into several levels depending on the magnitudes of each value as applied in the previous correlation analysis between the SOI and seasonal streamflow patterns. From the results of cross-correlation analysis for the total TNI phase, the resulting values of correlation coefficients are 0.03 (lag-1) to 0.05 (lag-4) for the entire stations over South Korea, −0.08 (lag-4) to 0.02 (lag-1) for El Niño core regions, and −0.12 (lag-1) to 0.13 (lag-1) for La Niña core regions, respectively. Consequently, the overall results from the above cross-correlation analysis indicate that the TNI is identified as not being significantly associated with seasonal streamflow in South Korea.

From the nonparametric test of the WRS test, a notable difference between both responses of streamflow fluctuation to the El Niño and La Niña forcing is identified at the 74% of confidence level. The results from the WRS test for both phases of ENSO phenomena suggest that the mean of the average signal season related to the El Niño episodes is stochastically different from, that is, greater than, that related to the La Niña episodes at the 90% confidence level.

An annual cycle diagram describing the relationship between the ENSO composites and streamflow fluctuation on a 3-year cycle basis is plotted in Figure 10 using modular coefficients through which streamflow time series are transformed into the proportion of original value to annual mean value for total records. It is evident from the annual cycle diagram plotted above that enhancement of streamflow for both core regions, for example, the HAN and NAK regions, are modulated by the El Niño forcing due to the fact that a period of consecutive months above annual cycle of streamflow variation for El Niño-related signal season is detected in the 3-year ENSO composite in Figure 10. In contrast, Figure 11 illustrates the comparison between 3-year La Niña composite and annual cycle of streamflow variation depending on the annual cycle diagram plotted by previously transformed modular coefficients. The resulting diagram shows that a period of persistent below normal streamflow anomalies for the La Niña-related signal season exists in the 3-year ENSO composite. Hence, it is plausible that suppression of streamflow for both core regions are modulated by the La Niña forcing. As an overall result of the inspection for the annual cycle diagrams, the warm ENSO forcing modulates streamflow variation by increasing, and the cold ENSO forcing modulates streamflow variation by decreasing its magnitude.

5 | DISCUSSIONS

As shown in Figures 4(a) and 5(a), the results of the present analyses indicate that below normal streamflow anomalies are observed in early autumn of El Niño year and above normal streamflow departures are observed from winter to spring of the ensuing year of the event over South Korea. In particular, the streamflow anomalies during September of the warm event year show predominant negative departures in comparison with that of the nonevent year. On the contrary, for La Niña event years, the exactly opposite tendency is observable as shown in Figures 7(a) and 8(a). The streamflow anomalies are above normal in early autumn of La Niña year and below normal from winter to spring of the ensuing year. Figure 12 illustrates the comparison of standard deviations for below (above) normal streamflow for September and above (below) normal streamflow from winter to spring during El Niño (La Niña) years using the seasonal streamflow data of both core regions. The points plotted for El Niño events are mostly distributed in the upper part of the left side, and those for La Niña events are oppositely distributed in lower part of the right side. These well-distinguishable distributions for both events represent the opposite tendency of

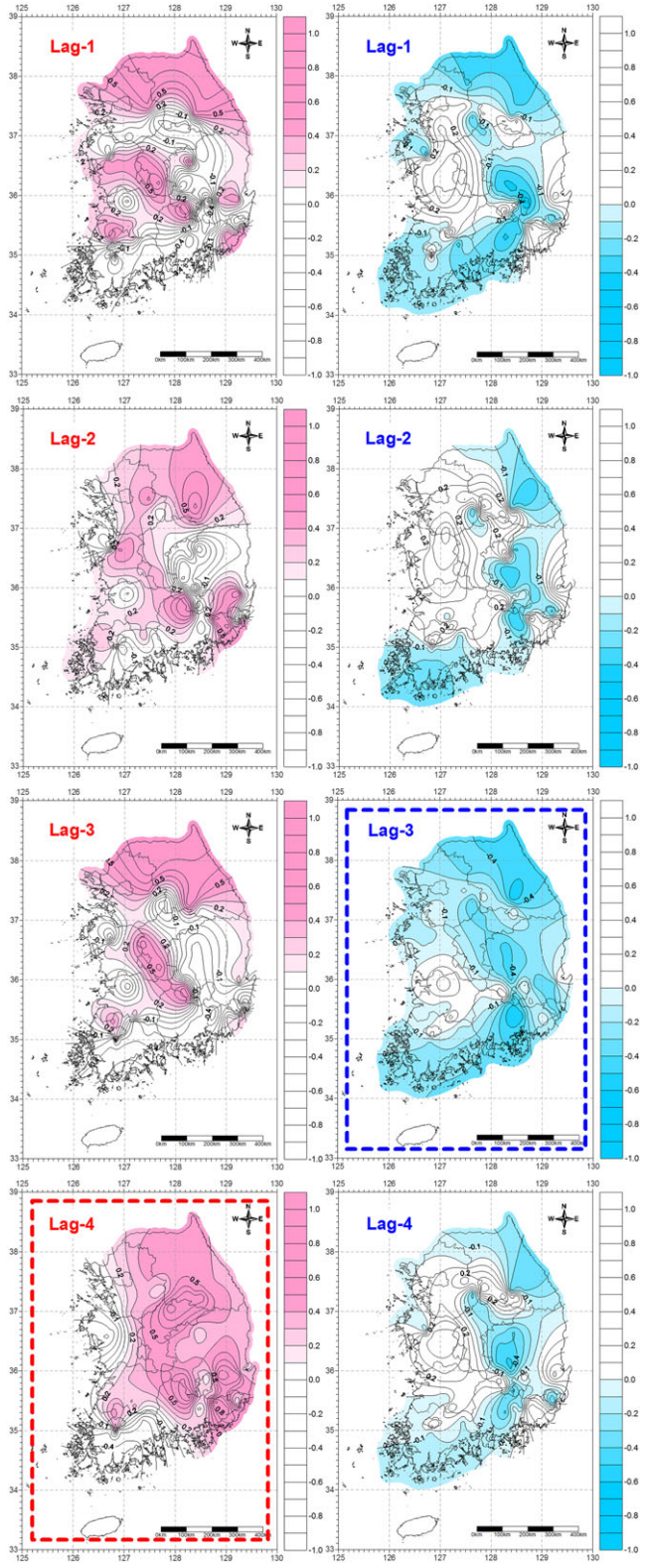

FIGURE 9 Spatial outlooks of correlation coefficients between the seasonal streamflow and the categorized Southern Oscillation index series at different lags for strong El Niño (left) and strong La Niña (right). The dashed boxes indicate correlations that are statistically most significant out of lag-1 to lag-4 based on the 90% confidence level. The nationwide values (the averaged values over all core regions) for strong El Niño lag-4 and strong La Niña lag-3 are 0.31 and −0.18 respectively

dry and wet anomalies of September and winter–spring season with respect to each extreme event.

In addition, in order to confirm the climatic teleconnections between large scale climate index and streamflow variability over South Korea, we calculated leading modes of observed monthly streamflow patterns through principal component analysis as well as demonstrated regression analysis for the leading modes and global sea surface temperature for extreme phase of the events. For global sea surface temperature, the Extended Reconstructed Sea Surface Temperature (ERSST.v4) dataset are employed in this study. The ERSST on a 2° × 2° grid basis is a global monthly SST dataset derived from the International Comprehensive Ocean–Atmosphere Dataset (ICOADS), which is suitable for long-term global and basin-wide studies. As shown in Figure 13, the results of the above analyses show that leading mode of winter–spring streamflow has a positive correlation with the tropical Pacific Ocean SSTs, while that of September streamflow shows a negative response to the tropical Pacific Ocean SSTs. These findings presented here can be considered as additional confirmation of aforementioned seasonal teleconnection between the tropical ENSO forcing and streamflow variability, which indicate drier (wetter) conditions in early autumn of the warm (cold) episode years and wetter (drier) conditions from winter to spring of the following year.

The physical interpretation of the influence of the extreme phase of ENSO on the midlatitude hydroclimatic parameters are difficult to construct. Over the western North Pacific, genesis and development of tropical cyclones play a crucial role in Korean precipitation and streamflow fluctuation during early autumn of the second rainy period. From the perspective of the above fact, it is plausible to seek some clue of remote climatic links in terms of the tropical storms and typhoons affecting overall streamflow basins in South Korea. Chu (2004) revealed that during the El Niño years, the eastward shift of monsoon trough having low-level cyclonic vorticity causes the mitigation of vertical wind shear over the western North Pacific. Cha et al. (1999) showed that the total number of typhoon generated throughout the western North Pacific decreases in the warm event years; furthermore, decrease (increase) of occurrences of tropical cyclones in the western North Pacific during the warm (cold) event years was examined by Li (1990). Consequently, the apparent decline in September streamflow is caused by the depression of the second rainy period by reduction of the tropical storms and typhoons over East Asia during the El Niño year, and increase of streamflow in September of the La Niña years is in association with the intensification of the second rainy period resulting from more frequent occurrences of tropical cyclones.

The Pacific-East Asia teleconnection, which was investigated by Wang, Wu, and Fu (2000), is a remote climatic link system between the central Pacific SST anomalies and the East Asia climate during the El Niño and La Niña years. From the perspective of the cyclone and anticyclone over the western North Pacific, the systematic configuration of the PEA teleconnection is considered as the lower tropospheric vorticity wave generated over the central Pacific with westward and poleward shift against the westerly jet stream. They indicated that the western North Pacific anomalous winds predominantly prevail and persist from late autumn to following

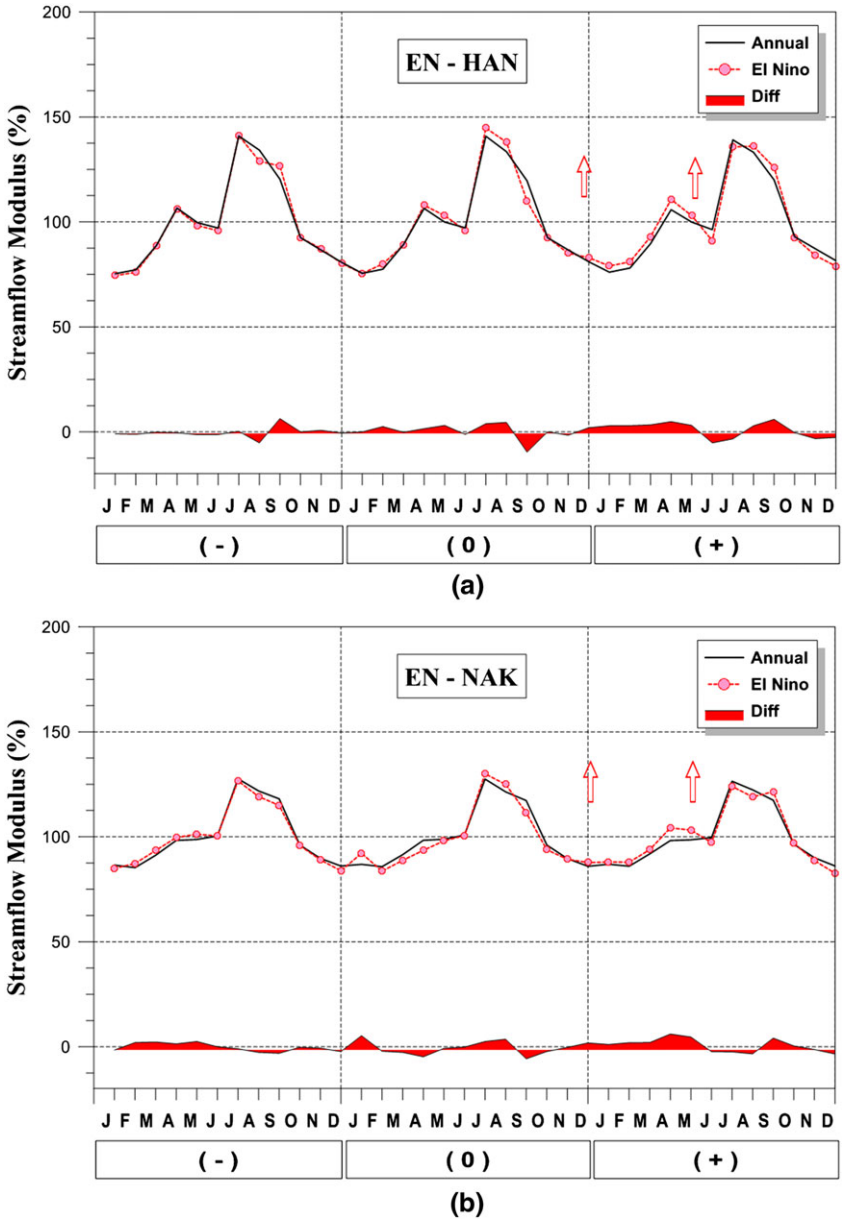

FIGURE 10 The comparison between El Niño composite cycles (shown by dashed line) and annual cycles (shown by solid line) of (a) the HAN region and (b) the NAK region, based on modular coefficients. Arrows indicate the beginning and end months of the Southern Oscillation signal season

winter–spring season during the mature phases of El Niño (La Niña), modulating increased (decreased) precipitation anomalies over East Asia by an enhanced (suppressed) winter monsoon. These features affect the amplification (depression) of winter to spring streamflow over South Korea during the warm (cold) phase of ENSO. As a result, above (below) normal streamflow departures are observed from winter to spring of the ensuing year of the El Niño (La Niña) event over South Korea.

The main focus of this analysis is to expand the previous global scale study of Ropelewski and Halpert (1987, 1989) by applying the empirical methodology to the streamflow patterns over a midlatitude region and to suggest new findings in South Korea located in East Asia. From the visual inspection of vectorial map plotted in the global scale study, it is worthwhile to note that there is no clear conclusive outcomes for East Asian region, as well as the ENSO-related signals over South Korea are not identified because of the limitation of data coverage, which is insufficient to examine the ENSO–streamflow teleconnection. Therefore, this present analysis expanded the previous studies through the use of a sufficient dataset covering the overall study area and by providing the spatial coherence map and the temporal consistency index for South Korea showing additional information on the ENSO-related signals over East Asian, which was not identified in the previous studies.

The overall results of these present analyses are in general agreement with those of several recent studies concerning the climatic impacts of the extreme phase of ENSO on hydroclimatic variables over South Korea. Cha et al. (1999) examined the climatic relationship between the remote ENSO forcing and Korean climatic variations such as precipitation, atmospheric circulation, temperature, and so on, and revealed that the El Niño (La Niña) events have a dominant impact on fluctuation of seasonal precipitation over South Korea modulating enhancement (suppression) of its magnitude. In a study on teleconnection between the tropical thermal forcing and Korean precipitation patterns using harmonic and correlation analysis, Lee and

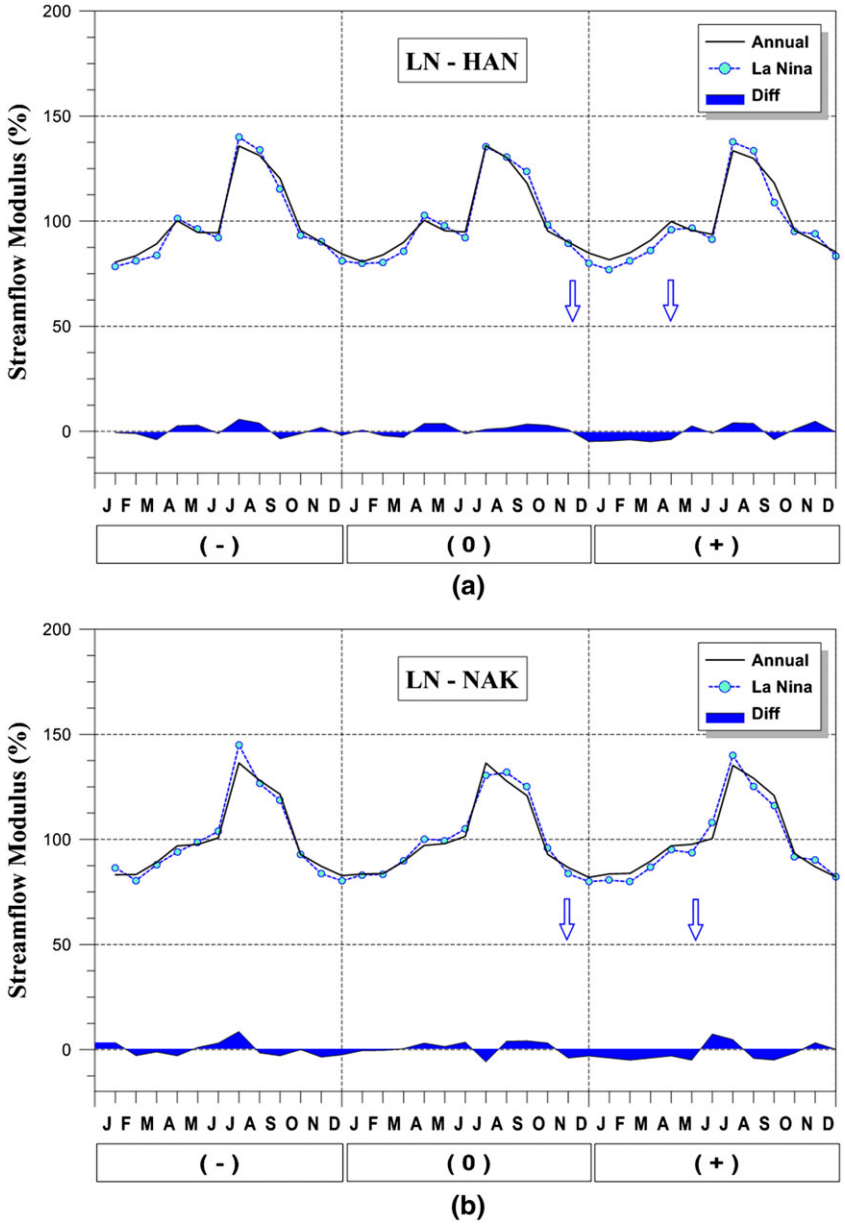

FIGURE 11 As in Figure 10, except for La Niña composite cycles

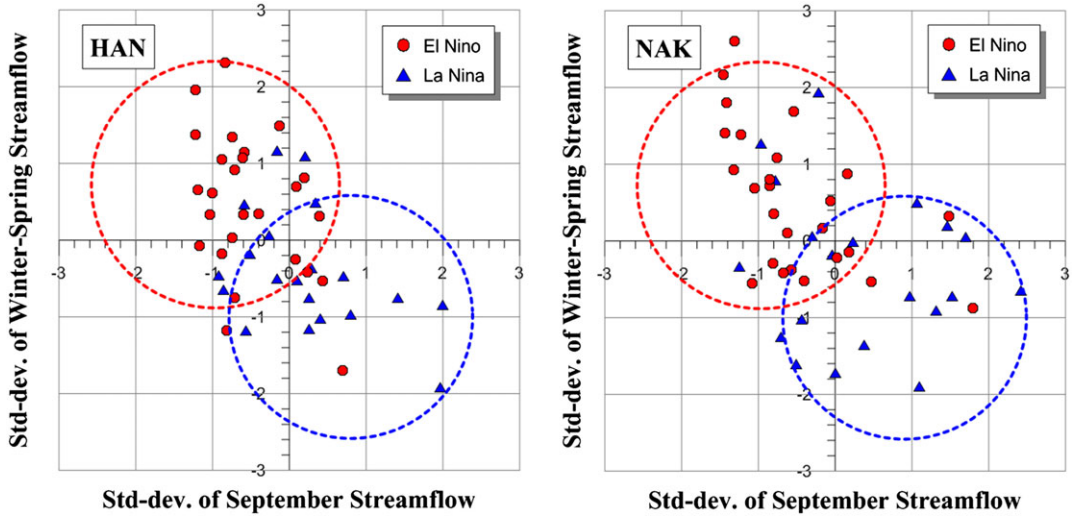

FIGURE 12 The comparison of standard deviations between below (above) normal streamflow in September and above (below) normal streamflow from winter through spring during El Niño (La Niña) events using the seasonal streamflow data of the HAN region (left) and the NAK region (right)

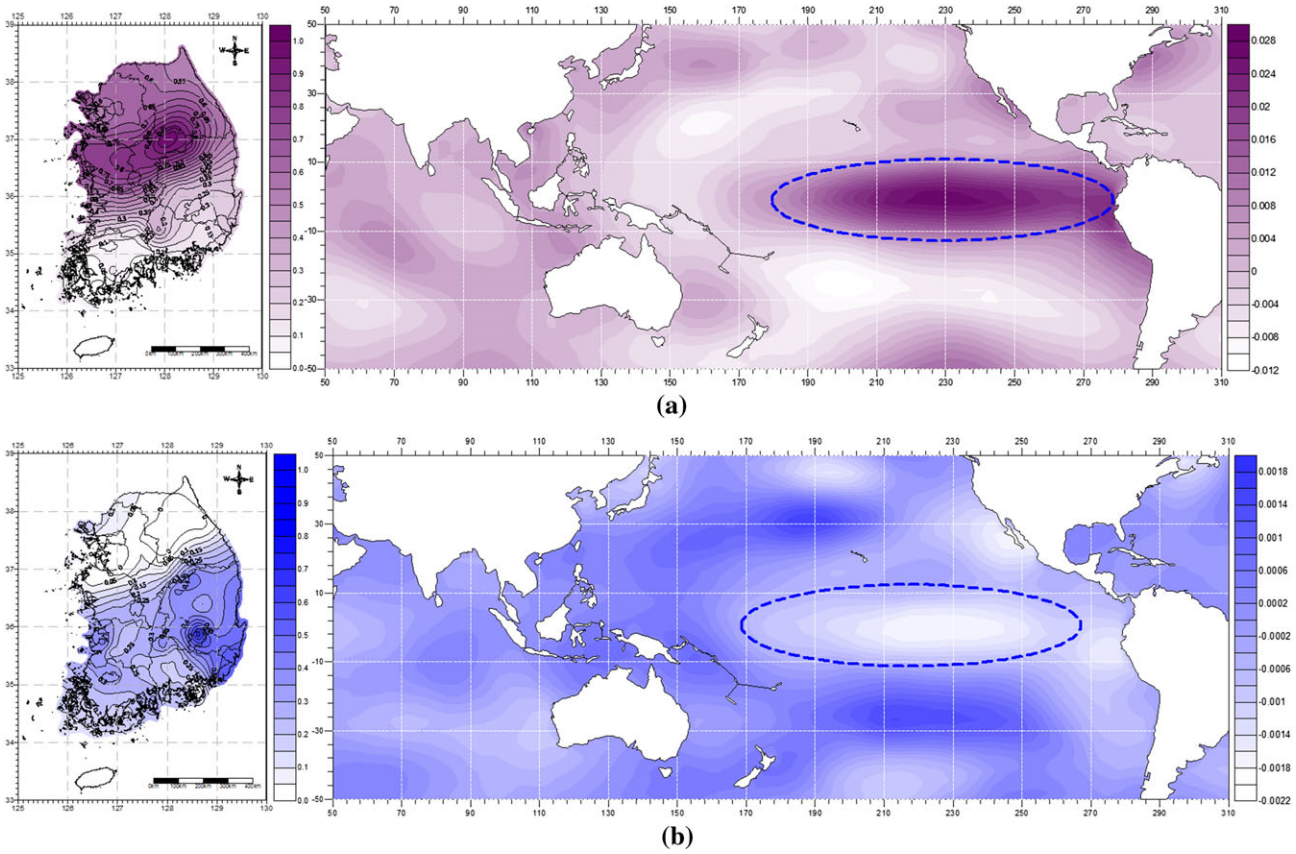

FIGURE 13 Spatial outlooks (left) of principal components of winter–spring (a) and September (b) precipitation based on central-point and regression coefficients of global sea surface temperatures (right) regressed on to leading mode for warm phase of El Niño/Southern Oscillation events

Julien (2015) indicated that the El Niño and La Niña events have a dominant impact on fluctuation of seasonal precipitation over South Korea. The results of their study can be summarized as follows. During the El Niño (La Niña) years, three (two) core regions were identified at over 94% (96%) of spatial coherence and 78% (82%) of temporal consistency with the overall signal seasons of November (0) to May (+), October (0) to May (+) for all core regions. In contrast, from specific findings of the present analysis, the overall signal seasons for the HAN and NAK regions during the El Niño (La Niña) years, are determined as December (0) to May (+), November (0) to May (+), showing 1 month lag response, which is caused by rainfall-runoff response time. Although there are some differences between the two studies, which are derived from the observational record period, gaging station coverages, and classification of candidate regions, this present analysis is consistent with and extends the previous investigation by Lee and Julien (2015). In addition, from a viewpoint of ENSO–streamflow signal seasons illustrated in the aggregate composite diagram for all core regions of this analysis, the driest (wettest) period of September is fairly coincident with the finding by Shin (2002) representing the suppression (enhancement) of early autumn precipitation during the warm (cold) extreme event years. The overall findings of aforementioned relevant studies are in general agreement with those of the present study. Consequently, in the light of the preceding discussions, the overall outcomes from the present analyses provide further confirmative evidence of the significant climatic teleconnection between the tropical ENSO forcing and hydroclimatic fluctuation over midlatitude.

6 | CONCLUSIONS

In the present study, the climatic teleconnections between warm or cold phases of ENSO and streamflow variations over South Korea are investigated based on an empirical methodology designed to detect regions showing a strong and consistent hydroclimatic signal associated with ENSO. From the composite-harmonic analysis, two core regions, that is, the Han river basin (HAN) and the Nakdong river basin (NAK), are detected with a high level of response of ENSO phenomena to streamflow variations. The overall results of the ENSO–streamflow teleconnections and specific findings of these analyses are summarized as follows.

During the warm event years, below normal streamflow anomalies are observed in early autumn of El Niño year and above normal streamflow departures are observed from winter to spring of the ensuing year of the event over South Korea. The signal season representing a strong and consistent ENSO–streamflow teleconnection, for the HAN region is the wet period of December (0) to May (+), and for the NAK region, January (+) to May (+). The spatial coherence rate (R_{sc}) and the temporal consistency rate (R_{tc}) are 92% and 71% for the HAN region, and 95% and 71% for the NAK region.

On the contrary, during the cold event years, the streamflow anomalies are above normal in early autumn of La Niña year and below normal from winter to spring of the ensuing year. The well-pronounced signal seasons for the dry condition are December (0) to April (+) for the HAN region and November (0) to May (+) for the NAK region resulting from the harmonic-composite analysis. The spatial coherence and temporal consistency rate are 82% and 75% for the HAN region, and 86% and 75% for the NAK region.

In addition, the results of comparative analyses by using correlation, annual cycle, and WRS test, indicate that two opposite phases-streamflow relationships have a tendency of sign reversal of the streamflow anomaly. Also, the positive departures during the El Niño years show more coherent and strong responses than the negative anomalies in the La Niña events. The results from the lag-correlation analysis indicate that the stronger the intensity of the extreme phase of ENSO, the larger the influence on South Korean streamflow fluctuation with the lag of 3 and 4 seasons. Also, the WRS test implies that the mean of the average signal season related to the El Niño episodes is stochastically greater than that related to the La Niña episodes. Moreover, the annual cycle diagrams suggest that the warm ENSO forcing modulates streamflow variation by increasing, and the cold ENSO forcing modulates streamflow variation by decreasing its magnitude. In conclusion, South Korea experiences climatic teleconnection between ENSO forcing and midlatitude streamflow patterns.

REFERENCES

Berlage, H. P. (1966). The Southern Oscillation and world weather. Meteor. Inst. Meded. Verh., 88, 152p.

Bradley, R. S., Diaz, H. F., Kiladis, G. N., & Eischeid, J. K. (1987). ENSO signal in continental temperature and precipitation records. *Nature*, *327*, 487–501.

Cayan, D. R., & Peterson, D. H. (1989). The influence of North Pacific atmospheric circulation on streamflow in the West, in aspects of climate variability in the Pacific and the Western Americas. *American Geophysical Union, Monograph*, *55*, 375–397.

Cayan, D. R., & Webb, R. H. (1992). El Niño/Southern Oscillation and streamflow in the western United States. In H. F. Diaz, & V. Markgraf (Eds.), *El Niño: Historical and Paleoclimatic aspects of the Southern Oscillation* (pp. 29–68). London: Cambridge University Press.

Cha, E. J., Jhun, J. G., & Chung, H. S. (1999). A study on characteristics of climate in South Korea for El Niño/La Niña years. *Journal of Korean Medical Science*, *35*(1), 99–117 (in Korean).

Chandimala, J., & Zubair, L. (2007). Predictability of streamflow and rainfall based on ENSO for water resources management in Sri Lanka. *Journal of Hydrology*, *335*, 303–312.

Chiew, F. H. S., McMahon, T. A., Dracup, J. A., & Piechota, T. (1994). El Niño/Southern Oscillation and the streamflow patterns in south-east Australia. *Civil Engineering Transactions, Institution of Engineers, Australia*, *CE36*(4), 285–291.

Chu, P. S. (2004). *ENSO and tropical cyclone activity* (pp. 297–332). New York: Columbia University Press.

Diaz, H. F., & Kiladis, G. N. (1993). El Niño/Southern Oscillation and streamflow in the western United States. In H. F. Diaz, & V. Markgraf (Eds.), *El Nitio: Historical and Paleoclimatic aspects of the Southern Oscillation* (pp. 8–28). London: Cambridge University Press.

Douglas, A. E., & Englehart, P. J. (1981). On a statistical relationship between autumn rainfall in the central equatorial pacific and subsequent winter precipitation in Florida. *Monthly Weather Review*, *109*, 2377–2382.

Dracup, J. A., & Kahya, E. (1994). The relationships between United States streamflow and La Nina events. *Water Resources Research*, *30*(7), 2133–2141.

Grimm, A. M., Ferraz, S. E. T., & Gomes, J. (1998). Precipitation anomalies in Southern Brazil associated with El Niño and La Niña events. *Journal of Climate*, *11*, 2863–2880.

Guttman, N. B. (1998). Comparing the Palmer drought index and the standardized precipitation index. *Journal of the American Water Resources Association*, *34*(1), 113–121.

Haan, C. T. (1977). *Statistical methods in hydrology*. Ames: Iowa State University Press 387p.

Horn, L. H., & Bryson, R. A. (1960). Harmonic analysis of the annual march of precipitation over the United States. *Annals of the Association of American Geographers*, *50*, 157–171.

Jin, Y. H., Kawamura, A., Jinno, K., & Berndtsson, R. (2005). Quantitative relationship between SOI and observed precipitation in southern Korea and Japan by nonparametric approaches. *Journal of Hydrology*, *301*, 54–65.

Kahya, E., & Dracup, J. A. (1993). US streamflow patterns in relation to the El Niño/Southern Oscillation. *Water Resources Research*, *29*(8), 2491–2503.

Kahya, E., & Dracup, J. A. (1994). The influences of Type 1 El Niño and La Niña events on streamflows in the Pacific southwest of the United States. *Journal of Climate*, *7*, 965–976.

Kahya, E., & Karabörk, M. C. (2001). The analysis of El Niño and La Niña signals in streamflows of Turkey. *International Journal of Climatology*, *21* (10), 1231–1250.

Karabörk, M. C., & Kahya, E. (2003). The teleconnections between extreme phases of Southern Oscillation and precipitation patterns over Turkey. *International Journal of Climatology*, *23*, 1607–1625.

Kashid, S. S., Ghosh, S., & Maity, R. (2010). Streamflow prediction using multi-site rainfall obtained from hydroclimatic teleconnection. *Journal of Hydrology*, *395*, 23–38.

Kennedy, A. M., Garen, D. C., & Koch, R. W. (2009). The association between climate teleconnection indices and upper Klamath seasonal streamflow: Trans-niño index. *Hydrological Processes*, *23*, 973–984.

Kiladis, G. N., & Diaz, H. F. (1989). Global climatic anomalies associated with extremes in the Southern Oscillation. *Journal of Climate*, *2*, 1069–1090.

Lee, D. R. (1999). Relationships of El Niño/Southern Oscillation and drought in Korea. *Journal of Korea Water Resources Association*, *312*(2), 111–120 (in Korean).

Lee, J. H., & Julien, P. Y. (2015). ENSO impacts on temperature over South Korea. *International Journal of Climatology*, *10*, 1002/4581.

Lee, J. H., & Julien, P. Y. (2016). Teleconnections of the ENSO and South Korean precipitation patterns. *Journal of Hydrology*, *534*, 237–250.

Li, C. (1990). On the interaction between anomalous circulation/climate in East Asia and El Niño event, climate change, dynamics and modelling. TISC August 12–20, pp. 101–126.

McKee, T. B., Doesken, N. J., & Kleist, J. (1993). The relationship of drought frequency and duration to time series. In *8th Conference on Applied Climatology*, Anaheim, CA, pp. 179–187.

Pan, Y. H., & Oort, A. H. (1983). Global climate variations connected with sea surface temperature anomalies in the eastern equatorial Pacific Ocean for the 1958-73 period. *Monthly Weather Review*, *111*, 1244–1258.

Price, C., Stone, L., Huppert, A., Rajagopalan, B., & Alpert, P. (1998). A possible link between El Niño and precipitation in Israel. *Geophysical Research Letters*, *25*, 3963–3966.

Quinn, W. H., Zopf, D. O., Short, K. S., & Kuo Yang, R. T. W. (1978). Historical trends and statistics of the Southern Oscillation, El Niño, and Indonesian droughts. *Fishery Bulletin*, *76*, 663–678.

Rasmusson, E. M., & Wallace, J. M. (1983). Meteorological aspects of the El Niño/southern oscillation. *Science*, *222*, 1195–1202.

Redmond, K. T., & Koch, R. W. (1991). Surface climate and streamflow variability in the western United States and their relationship to large circulation indices. *Water Resources Research*, *27*(9), 2381–2399.

Ropelewski, C. F., & Halpert, M. S. (1986). North American precipitation and temperature patterns associated with El-Niño-Southern oscillation (ENSO). *Monthly Weather Review*, *114*, 2165–2352.

Ropelewski, C. F., & Halpert, M. S. (1987). Global and regional scale precipitation patterns associated with the El Niño/Southern oscillation. *Monthly Weather Review*, *115*, 1606–1626.

Ropelewski, C. F., & Halpert, M. S. (1989). Precipitation patterns associated with the high index phase of the southern oscillation. *Journal of Climate*, *2*, 268–284.

Schonher, T., & Nicholson, S. E. (1989). The relationship between California rainfall and ENSO events. *Journal of Climate*, *2*, 1258–1269.

Scott, C. M., & Shulman, M. D. (1979). An areal temporal analysis of precipitation in the Northeastern United States. *Journal of Applied Meteorology*, *18*, 627–633.

Shin, H. S. (2002). Do el Niño and La Niña have influences on South Korean hydrologic properties? In *Proceedings of the 2002 Annual Conference, Japan Society of Hydrology and Water Resources*, pp. 276–282.

Stoeckenius, T. (1981). Interannual variations of tropical precipitation patterns. *Monthly Weather Review*, *109*, 1233–1247.

Trauth, M. H. (2015). *Matlab recipes for earth sciences* (Fourth ed.) (pp. 103–109). Heidelberg: Springer.

Trenberth, K. E. (1997). The definition of El Niño. *Bulletin of the American Meteorological Society*, *78*, 2771–2777.

Trenberth, K. E., & Stepaniak, D. P. (2001). Indices of El Niño evolution. *Journal of Climate*, *14*, 1697–1701.

Walker, G. T. (1923). Correlation in seasonal variations of weather, V III, a preliminary study of world weather. *Memoirs of the India Meteorological Department*, *24*, 75–131.

Wang, B., Wu, R., & Fu, X. (2000). Pacific–East Asian teleconnection, how does ENSO affect east Asian climate. *Journal of Climate*, *13*, 1517–1536.

Wilks, D. S. (1995). *Statistical methods in atmospheric sciences* (pp. 330–334). San Diego: Academic Press.

Zhang, Q., Xu, C. Y., Jiang, T., & Wu, Y. (2007). Possible influence of ENSO on annual maximum streamflow of the Yangtze River, China. *Journal of Hydrology*, *333*, 265–274.

How to cite this article: Lee JH, Julien PY. Influence of the El Niño/Southern Oscillation on South Korean streamflow variability. *Hydrological Processes*. 2017. https://doi.org/10.1002/hyp.11168